PROTEINS: Structure, Function, and Genetics 46:225–234 (2002)

Structure of Met-Enkephalin in Explicit Aqueous Solution Using Replica Exchange Molecular Dynamics

K.Y. Sanbonmatsu* **and A.E. García**
Los Alamos National Laboratory, Los Alamos, New Mexico

ABSTRACT **Replica exchange molecular dynamics (MD) simulations of Met-enkephalin in explicit solvent reveal helical and nonhelical structures. Four predominant structures of Met-enkephalin are sampled with comparable probabilities (two helical and two nonhelical). The energy barriers between these configurations are low, suggesting that Met-enkephalin switches easily between configurations. This is consistent with the requirement that Met-enkephalin be sufficiently flexible to bind to several different receptors. Replica exchange simulations of 32 ns are shown to sample approximately five times more configurational space than constant temperature MD simulations of the same duration. The energy landscape for the replica exchange simulation is presented. A detailed study of replica trajectories demonstrates that the significant increases in temperature provided by the replica exchange technique enable transitions from nonhelical to helical structures that would otherwise be prevented by kinetic trapping. Proteins 2002;46:225–234.** © 2001 Wiley-Liss, Inc.*

Key words: molecular dynamics; opioid; energy landscape; kinetic trapping; protein folding; parallel computing

INTRODUCTION

Met-enkephalin (YGGFM) is an opioid peptide that inhibits neurotransmitter release upon activation of the appropriate opioid receptor.[1,2] Opioid peptides play a significant role in pain mediation, opiate dependence, and euphoria[3,4] and have aromatic residues in positions 1 and 4. Opioid systems have been shown to regulate dopamine release[3] and are thought to be central to drug-induced reward.[5] Despite numerous studies over the past 25 years in nuclear magnetic resonance (NMR),[4] infrared (IR),[6] ultraviolet (UV),[7] circular dichroism (CD),[8,9] fluorescence,[10] and x-ray crystallography,[11] no unique native structure has been determined for Met-enkephalin. This short peptide binds to either the μ-, κ-, or δ-receptor, depending on the biological context, requiring it to be flexible enough to take on several different conformations.[2] This flexibility has led to conflicting experimental evidence for the structure. NMR studies of Met-enkephalin in sodium dodecyl sulfate (SDS) micelles show distinct ordering of conformation. However, these same studies have concluded that conformations of Met-enkephalin in aqueous solution demonstrate poor convergence to a single structure.[4] Because of the lack of distinct structures observed for Met-enkephalin, many studies have been performed for synthetic analogues, such as [D = Pen2, D-Pen5] enkephalin (DPDPE), and display significantly greater structural stability, producing cyclic conformations with disulfide bridges.[12] The structure of Met-enkephalin itself, however, remains ill-defined.

Many standard molecular dynamics (MD) simulations of Met-enkephalin, as well as Monte Carlo simulations,[15–17] have been performed.[13,14] The MD simulations, some with explicit solvent, evolve the peptide at a single temperature and are known to suffer from kinetic trapping, where inadequate sampling confines the peptide to artificial configurations. Recently, multicanonical methods have been developed that enable the peptide to achieve greater sampling of energy space, decreasing the effects of kinetic trapping.[18–20] The multicanonical methods have been applied to Met-enkephalin, using implicit solvent models.[17] A similar method, simulated tempering, allows the system to sample greater regions of temperature space.[21,16] This method has generally been used in Monte Carlo simulations; however, this technique was recently applied to MD simulations and adapted to run effectively on parallel computers.[22] This adaptation, termed replica exchange MD, has the additional advantage of near-linear scaling of simulation time speedup with processor number resulting from the minimal communication time required between processors. This scaling represents a significant advance in light of the poor scaling of standard MD simulation codes with respect to the processor number for large numbers of processors.[23]

In the replica exchange method, copies of the peptide system, identical except for temperature, exchange temperatures after a given time interval, avoiding kinetic traps by sampling high temperatures. This temperature sampling facilitates barrier crossings on the energy landscape (i.e., transitions between stable configurations), creating trajectories well suited for detailed investigation of the mechanism of configurational transitions.

Previously, replica exchange MD was implemented for Met-enkephalin in vacuum[22] and the GB1 β-hairpin in explicit aqueous solution.[24] In light of recent studies

Grant sponsor: United States Department of Energy; Grant contract: W-740-ENG-36; Grant sponsor: Los Alamos National Laboratory.

*Correspondence to: Kevin Y. Sanbonmatsu, MS B259, Los Alamos National Laboratory, Los Alamos, NM 87545. E-mail: kys@lanl.gov

Received 15 December 2000; Accepted 6 July 2001

DOI 10.1002/prot.0000

demonstrating the importance of explicit solvent,[25–28] this article presents replica exchange MD simulations of Met-enkephalin in explicit aqueous solution. We attempt to understand the structure of Met-enkephalin and its implications for biological function. Met-enkephalin also presents a useful system for the study of peptide folding, allowing us to examine local folding transitions in great detail.

Sugita's replica exchange methods is presented, along with the details of the preparation of the solvated Met-enkephalin, followed by the configurational analysis and energy landscape. The transition between stable structures of Met-enkephalin is also investigated. The replica exchange MD results are compared with the results of a control system, using constant temperature molecular dynamics at $T = 300$ K. Finally, the implications of our results for the structure and function of Met-enkephalin are discussed in light of previous work.

METHODS

Replica Exchange Algorithm

The replica exchange MDs algorithm[22] evolves several copies of a system, each using a separate process. The copies, or replicas, are identical, with the exception of their temperature. A distribution of target temperatures $(T_1, \ldots, T_i, T_j, \ldots, T_{M_{\text{proc}}})$ is chosen for M_{proc} replicas, whose coordinates are represented by $q_1, \ldots, q_m, q_n, \ldots, q_{M_{\text{proc}}}$. Initially, $i = m$ and $j = n$. The replicas are advanced in time until they reach their respective target temperatures via temperature coupling. At this point, each replica attempts to exchange temperatures with another replica system, using the Monte Carlo criterion:

$$P(\text{exchange}) = \exp[1/kT_i - 1/kT_j)(E(q_m) - E(q_n)] \quad (1)$$

If eq. 1 is satisfied, the replica systems exchange target temperatures, such that $T(q_i) = T_n$ and $T(q_j) = T_m$. This is the only time during the simulation when processors communicate. The exchanging replicas are subsequently advanced for a longer period of time than it takes to reach their new target temperature by coupling to the heat bath. All other replicas are also evolved for the same amount of time, at which point another set of exchanges is attempted. Because the number of timesteps between exchange attempts is much greater than unity, the communication requirements of this method are minimal, resulting in near-linear scaling of speedup with processor number. Upon inspection of eq. 1, it is obvious that only replicas with neighboring target temperatures will have significant exchange probabilities. This fact prompts us to attempt only exchanges between neighboring (in temperature) replicas. By successively exchanging target temperatures with neighboring replica systems, a given replica may sample a wide range of temperatures.

Preparation

The Met-enkephalin peptide ($AcYGGFMNH_2$) was modeled using the Cornell et al.[29] force field PARM94 and the AMBER suite of simulation codes.[30] The peptide was solvated in the linear conformation using the Tip3p water model[29] with approximately 600 water molecules. Periodic boundary conditions were enforced using the minimum image method. Long-range forces were truncated with a 9-Å cutoff, which is reasonable for short peptides that lack charged residues for sufficiently large box sizes. This system of explicit water and one Met-enkephalin molecule was minimized using the steepest decent method and was subsequently equilibrated at constant pressure (1 atm) and temperature ($T = 300$ K), using the Berendsen algorithms[31] ($\tau_T = 0.1$ ps and $\tau_P = 0.2$ ps) for 200 ps with a timestep of 2 fs. A system density of ≈ 1 g/cm^3 was obtained, corresponding to a cube of edge length $L \approx 26.62$ Å. The system was then equilibrated further at constant (N, V) for 100 ps.

To determine the distribution of target temperatures for the replicas, the resulting system was equilibrated at four different temperatures, $T = 275$, 325, 375, and 450 K. From these, the average energies E were obtained, allowing us to fit $E(T)$ with a polynomial. Finally, eq. 1 was solved iteratively for the temperature distribution using $P(\text{exchange}) = 0.20$, chosen to produce ample exchanges between replicas, while simultaneously providing good overlap of energy histograms of replicas adjacent in temperature. The resulting temperature distribution is $T =$ 275, 282, 289, 296, 305, 313, 322, 331, 340, 350, 360, 371, 382, 394, 406, 419 K. Sixteen copies of the above system (i.e., the system equilibrated at $T = 300$ K) were generated and equilibrated separately at the above 16 temperatures for 150 ps at constant (N, V, T). The time between exchanges (during the production stage) was chosen to ensure sufficient time for the system to couple to the heat bath, i.e., $t_{\text{exch}} > \tau_{\text{solv}}$.

Production

The replica exchange MD algorithm of Sugita and Okamoto[22] was implemented on an eight CPU LINUX cluster using two processes per processor. The above ensemble of 16 systems of Met-enkephalin in explicit water was evolved via replica exchange MD for 2 ns, using the exchange criterion (eq. 1), yielding a total sampling of 2 ns $\times$ 16 replica = 32 ns. A control system consisting of one solvated Met-enkephalin system at constant (N, V, T) with $T = 300$ K was simulated for 32 ns, using constant temperature MD. This system used the same initial configuration as that used to generate the replica systems described above.

RESULTS

Replica Exchange Diagnostics

Figure 1 displays the temperature evolution of 4 of the 16 replicas, demonstrating that the replicas sample a wide range of temperatures. The other 12 replicas sample similar ranges of temperatures. The first 150 ps display the equilibration period before replicas were permitted to exchange temperatures. The exchange of target temperatures for all replicas is shown in detail for the first 25 ps of replica exchange in Figure 2. The average exchange rate (i.e., the ratio of the number of successful exchanges to the number of exchange attempts) was approximately 22.5%. The configurations of all replicas were sorted according to

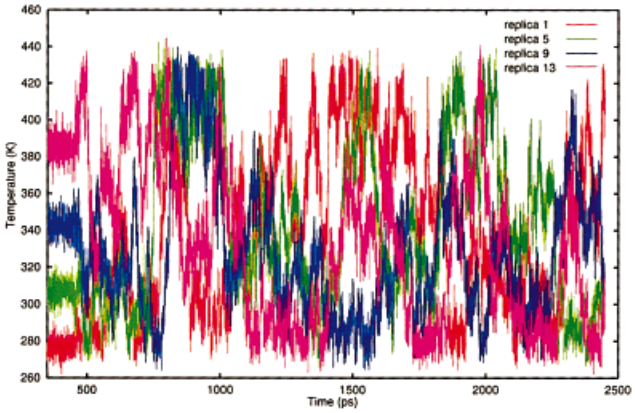

Fig. 1. Temperature evolution of 4 of the 16 replicas. The replicas sample a wide range of temperatures.

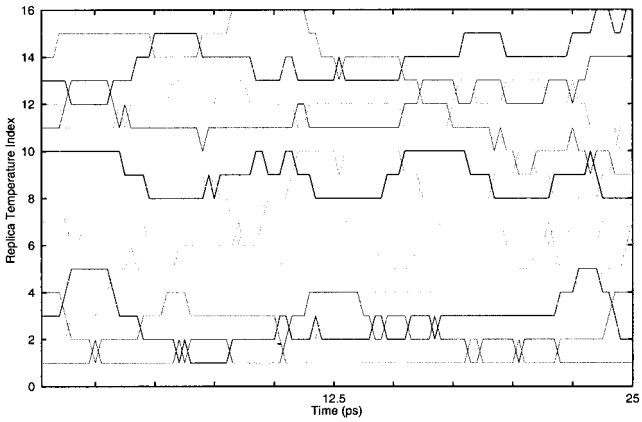

Fig. 2. Index of the target temperature for each replica versus time. Only replicas with neighboring target temperatures exchange target temperatures.

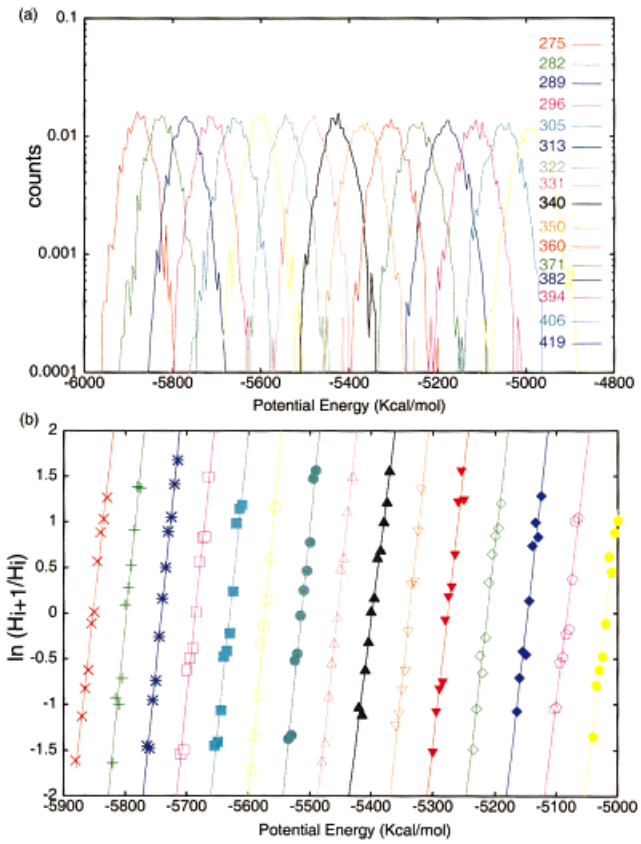

Fig. 3. **a:** Energy histograms of replicas produced by sorting configurations according to target temperature. Significant overlap permits successful exchange of target temperatures. **b:** Ratio of histograms $\log[H(E, T_{i+1})/H(E, T_i)]$ (symbols) and least-squares fit to corresponding Boltzmann distributions (solid curves), demonstrating that equilibrium is achieved.

target temperature. The energy histograms, $H(E, T)$, of each target temperature show significant overlap, ensuring a relatively high rate of exchange and substantial sampling over a wide range of energies (Fig. 3a). We use Bennet's method of energy histogram overlap to verify that out simulations are sampling from a Boltzmann distribution. The ratio of energy histograms over the energy range for which there is significant overlap must satisfy:

$$\log[H(E, T_2)/H(E, T_1)] = (1/k_B T_1 - 1/k_B T_2)E + \text{const}$$

Figure 3b displays the ratios of neighboring histograms along with corresponding least-squares fits to ratios of Boltzmann distributions. The Boltzmann distributions fit the simulation data to within the statistical error (<5%), showing that equilibrium (i.e., Boltzmann sampling) is achieved.

Configurational Sampling

Ramachandran plots depicting the sampling of (ϕ, ψ) dihedral angle space for all replicas and all temperatures are shown in Figure 4 for the five residues of Met-enkephalin. Contours of $\ln(M/M_{\text{tot}})$ are shown, where M is the number configurations with a particular (ϕ, ψ) and $M_{\text{tot}} = 1.28 \times 10^5$ is the total number of configurations. The data were smoothed using boxcar smoothing (i.e., convolving the data set with a top-hat function of finite width) to elucidate larger features present amidst many small fluctuations. All five residues sample the region of (ϕ, ψ) space corresponding to α-helices. Tyr 1, Phe 4, and Met 5 have particularly pronounced coverage of this region, showing two regions of sampling, near (ϕ, ψ) $\approx$ (-135, -30) and (ϕ, ψ) $\approx$ (-85, -30), corresponding to the α_R and α' conformations.[32,33]

Tyr 1, Phe 4, and, to some extent, Met 5, also sample the β hairpin region of (ϕ, ψ) space. The L region (left-handed α-helix) is sampled by Gly 2, Gly 3, and Phe 4. Figure 5 superimposes contours for all five residues, explicitly illustrating that all residues sample the α-helix region and that several sample β hairpin dihedral angles. A similar structure in (ϕ, ψ) space has been observed in NMR and MD studies of [Met5]enkephalin-Arg-Phe, which provide Ramachandran plots for Gly 3 and Phe 4.[9] The Ramachandran plots for our simulations and those of the [Met5]enkephalin-Arg-Phe studies contrast with studies of Leu-enkephalin,[34] which show little sampling of α-helix regions for Gly 2 and Gly 3 and little sampling of β hairpin regions for Phe 4.

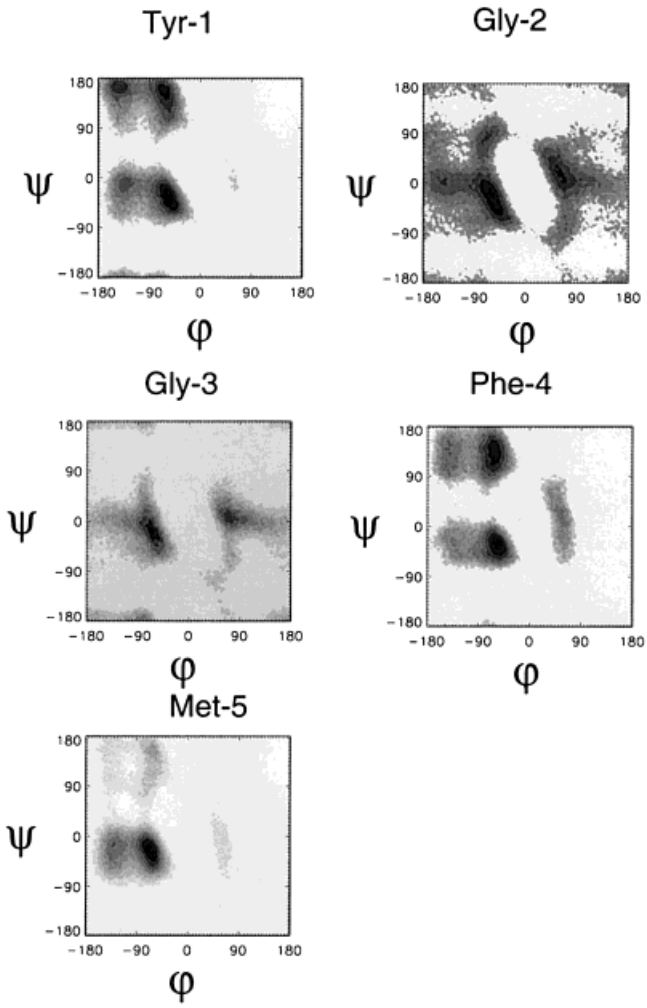

Fig. 4. Ramachandran plots for all five residues of Met-enkephalin, using the PARM94 force field.

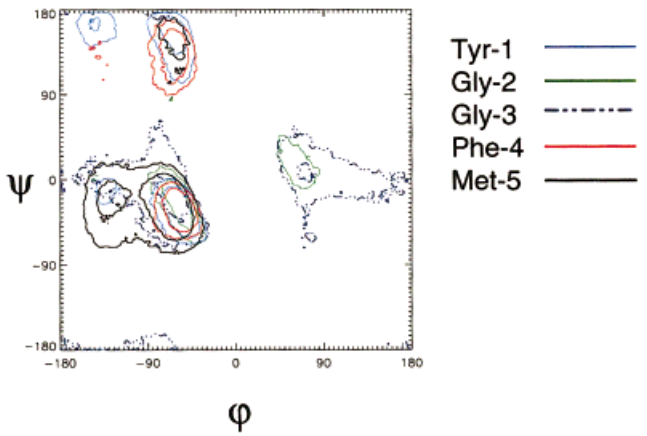

Fig. 5. ϕ, ψ contours of all five residues of Met-enkephalin superimposed.

Principal component analysis is used for systematic visualization of the conformational sampling of all residues simultaneously.[35,36] Each configuration of Met-enkephalin is represented by a point in 3N-dimensional space, $\mathbf{r}_i \in \mathbf{R}^{3N}$, where N is the number of atoms in the peptide. The principal component space is determined by finding a basis set, $\{\hat{\mathbf{a}}_1, \ldots, \hat{\mathbf{a}}_{3N}\}$, and reference configuration, $\mathbf{r}_0$, which minimize the mean square distance d of all configurations and the reference configuration,

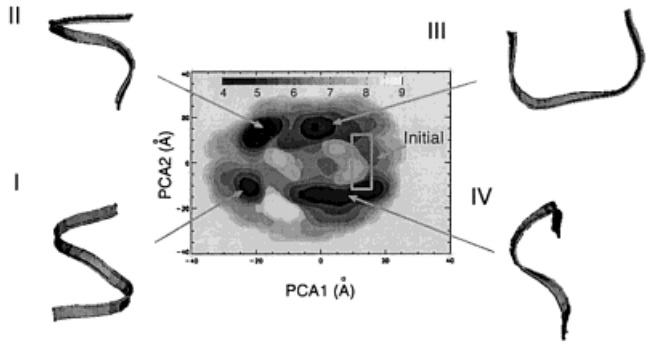

Fig. 6. Principal component analysis for all replicas at $T = 275$ K. Ribbon renderings of the backbone of the four predominant configurations are shown (generated using VMD visualization software[37]), along with the region of *PCA* space corresponding to the initial conditions for the various replicas (rectangle).

$$d^2 = \frac{1}{M_{\text{tot}}} \sum_{i=1}^{M_{\text{tot}}} (\mathbf{r}_i - \mathbf{r}_0)^2 + [(\mathbf{r}_i - \mathbf{r}_0) \cdot \hat{\mathbf{a}}_i)^2 \qquad (2)$$

The reference configuration that minimizes eq. 2 is the average configuration, i.e., $\mathbf{r}_0 = \langle \mathbf{r} \rangle$. The basis set that minimizes eq. 2 is the basis on which the average projection of all configurations is minimized. The principal component basis $\{\hat{\mathbf{e}}_1, \ldots, \hat{\mathbf{e}}_n\}$ is determined by finding the basis orthogonal to $\{\hat{\mathbf{a}}_1, \ldots, \hat{\mathbf{a}}_n\}$. The first principal component basis vector (corresponding to the largest eigenvalue of the eigenvalue equation used to determine the principal component basis) is that which maximizes the projection of $\langle \mathbf{r} \rangle$. Each configuration can be represented by

$$\mathbf{r}_i = \sum_{i=1}^{M_{\text{tot}}} p_i \hat{\mathbf{e}}_i \qquad (3)$$

where p_i are the projections onto the principal component basis.

Figure 6 displays contours (smoothed using boxcar smoothing) of the potential of the mean force of the configurations of all replicas with target temperatures $T = 275$ K, projected onto the first two principal component basis vectors. The potential of mean force is given by $W/kT = -\ln(M/M_{\text{tot}})$. The potential of mean force surface shows four major basins whose minima correspond to the four structures shown in Figures 6 and 7. The rectangle encompasses the initial configurations of all replicas. Structure I (Fig. 7a) is an α-helix structure, containing three α-helix hydrogen bonds between the acetate end group and Phe 4, Tyr 1, and Met 5, and between Gly 2 and the methylamine end group. Structure II (Fig. 7b) has only one hydrogen bond (between Gly 2 and the methylamine end group), yet is still generally helical. The backbone of structure III (Fig. 7c) is nonhelical, forming a two-dimensional U shape, with a hydrogen bond forming

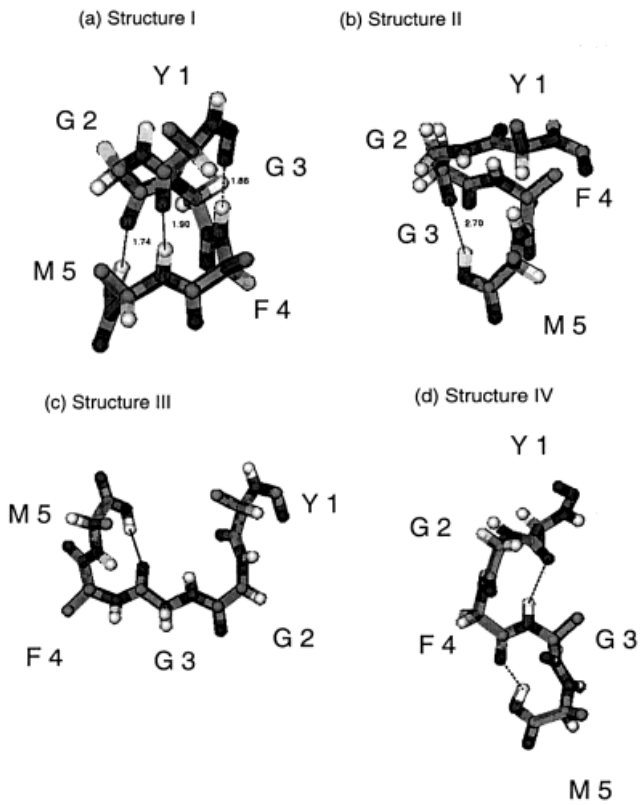

Fig. 7. Backbone renderings of the four predominant configurations of Met-enkephalin (generated using VMD visualization software[37]). Hydrogen bonds are depicted by dashed lines.

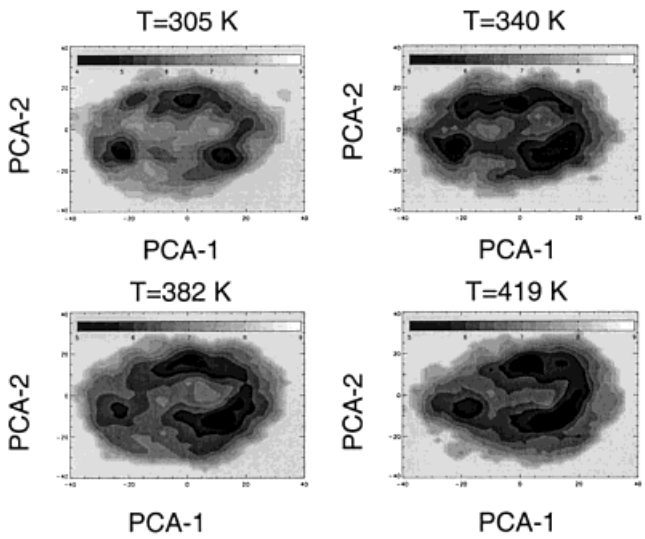

Fig. 8. Potential of mean force contours for all replicas with target temperatures $T = 305$ K, $T = 340$ K, $T = 382$ K, and $T = 419$ K.

between the methylamine end group and Gly 3. Structure IV (Fig. 7d) is also nonhelical and has a β-hairpin hydrogen bond between Tyr 1 and Phe 4, explaining the large amount of sampling of the β-hairpin region of (ϕ, ψ) space shown in Figure 4.

The potential of mean force contours for $T = 305$ K, $T = 340$ K, $T = 382$ K, and $T = 419$ K are displayed in Figure 8. The basins corresponding to structures II and III merge with increasing temperature. By $T = 419$ K, basin IV begins to merge with basins II and III, while basin I (corresponding to the α-helix) remains intact.

Energy Landscape

Figure 9a displays the potential of mean force surface on the (*PCA*-1, *T*) plane, illustrating explicitly that replica MD enables sampling in temperature space. This surface shows two major basins corresponding to the helical (i.e., structures I and II) and nonhelical (i.e., III and IV) structures, respectively. The helical basin has $PCA\text{-}1 \approx -20$ Å and is slightly deeper than the nonhelical basin. The nonhelical basin is relatively broad, covering the region $-20 < PCA\text{-}1 < 0$. The surface is rugged, although the large barrier between the two basins tends to decrease with increasing temperature, depicted more clearly in Figure 9b, which shows the same surface from a different vantage point. The relative populations of the nonhelical and helical basins are shown in Figure 10 as a function of target temperature. Note that the populations are normalized to the number of samples at a particular target temperature, as opposed normalization by the total number samples used in Figure 9. Although the energy minimum of the helical basin is lower than that of the nonhelical basin, configurations in the nonhelical basin are sampled at a higher frequency because the nonhelical basin is substantially wider. The lack of variation in the populations indicates that the coexistence of the two populations is disordered and uncooperative. Furthermore, since the barrier between the two basins is on the order of $\approx kT$, the peptide may move easily between basins. This is consistent with the ability of Met-enkephalin to bind to several different receptors.

Transition Trajectories

This section follows the transition of a single replica (replica 9) from the nonhelical to helical basin. Rather than making the transition at the highest temperature ($T = 419$ K) in the target temperature distribution, this replica makes the transition near $T \approx 340$ K as a result of the relative minimum near ($PCA\text{-}1$, T) $\approx$ (-10 Å, 340 K) on the potential of mean force surface (shown in Fig. 9b). This is shown explicitly in Figure 11a, which shows the approximate trajectory of replica 9 in (*PCA*-1, *T*) space, superimposed on the configurations (represented by single points) of all replicas at all temperatures. The crossing from the nonhelical to helical basin occurs near $T \approx 340$ K. Only every 1250th configurational point is shown, so that the trajectory of replica 9 may be seen more clearly (red). Every 12500th point of the trajectory of replica 9 is shown to convey the overall motion in (*PCA*-1, *T*) space (black solid curve). Figure 11b depicts the trajectory of the same replica in (*PCA*-1, *PCA*-2) space. The peptide begins in structure IV and quickly changes to structure III. After remaining in structure III for some time, the peptide briefly moves through the basin in (*PCA*-1, *PCA*-2) space corresponding to structure IV on its way to structure I, where it

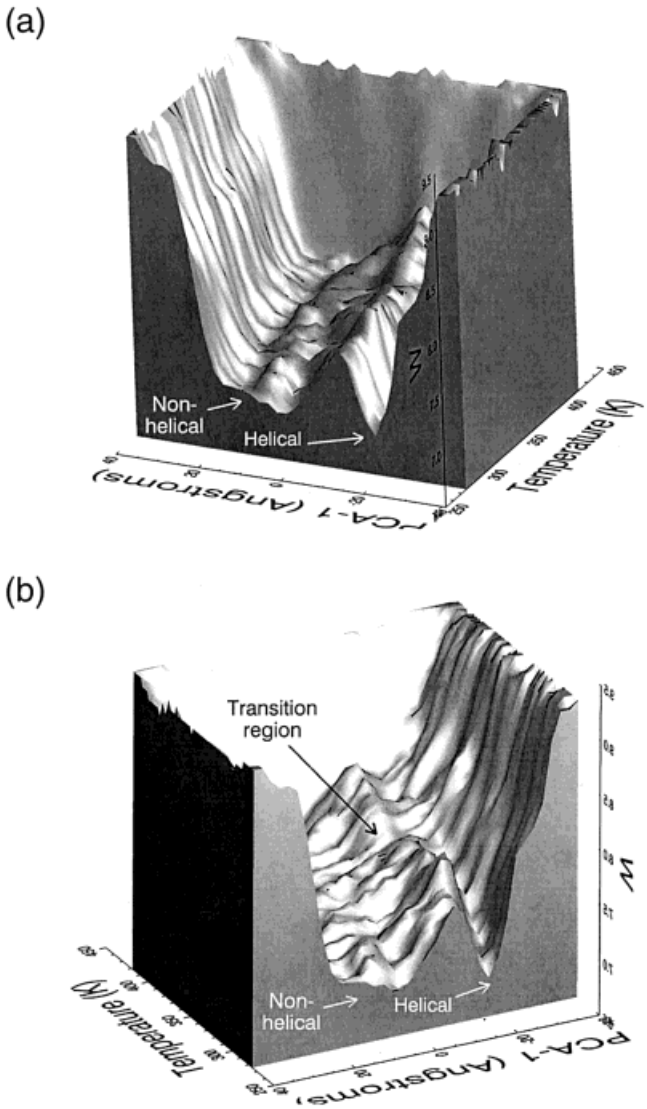

Fig. 9. **a:** Energy landscape of Met-enkephalin. **b:** Energy landscape of Met-enkephalin from a vantage point at which the transition region is observable.

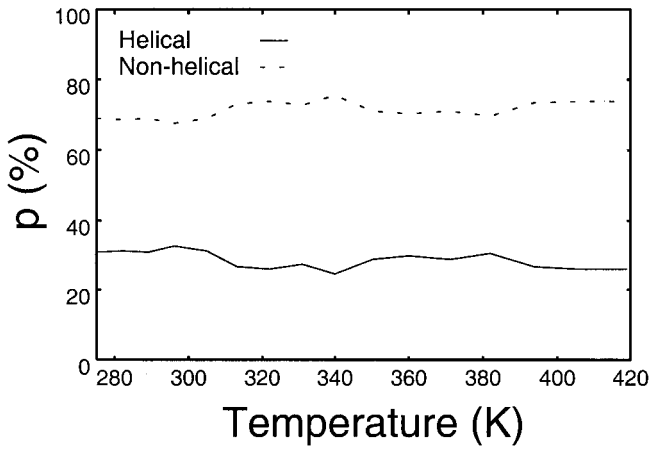

Fig. 10. Relative populations of the helical and nonhelical basins in the energy landscape as a function of target temperature.

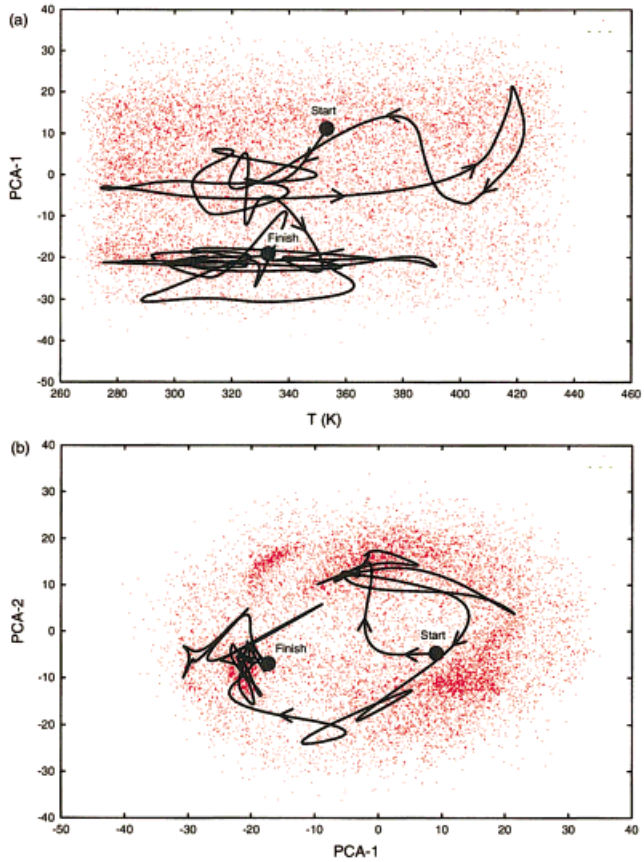

Fig. 11. **a:** Trajectory of replica 9 superimposed on (*PCA*-1, *T*) space configurations for all replicas. **b:** Trajectory of replica 9 superimposed on (*PCA*-1, *PCA*-2) space configurations for all replicas.

stays for the remainder of the simulation. From the trajectory of this single replica, it appears that structures III (U-shaped) and I are more stable structures, while the structure IV represents a transition configuration between III and I. That is, the transition follows the pathway, III (U-shaped) → IV → I (helical).

In its transition to the α-helix structure I, the backbone of the U-shaped structure III undergoes simultaneous torsional and compressional deformations. This is demonstrated in Figures 12 and 13, which display the time series of structures during the transition using VMD software.[37] Figure 12 shows the backbone in ribbon rendering along with Tyr 1, Phe 4, and the NME terminus. The coordinate axes shown are co-moving with the molecule. The perspective is most easily understood by referring to the α-helix structure in Figure 12f, which shows the profile view of the helix. The *z*-axis is parallel to the axis of the helix. Figure 13f shows the helix looking down its axis. Again, the *z*-axis is parallel to the axis of the helix.

The torsional deformation is exhibited between t = 960 ps and t = 994.75 ps. Although not obvious from Figure 12a,b, this is clear upon inspection of Figure 13a,b. Because the front and rear arms (corresponding to the left and right arms in Figure 12a, respectively) of

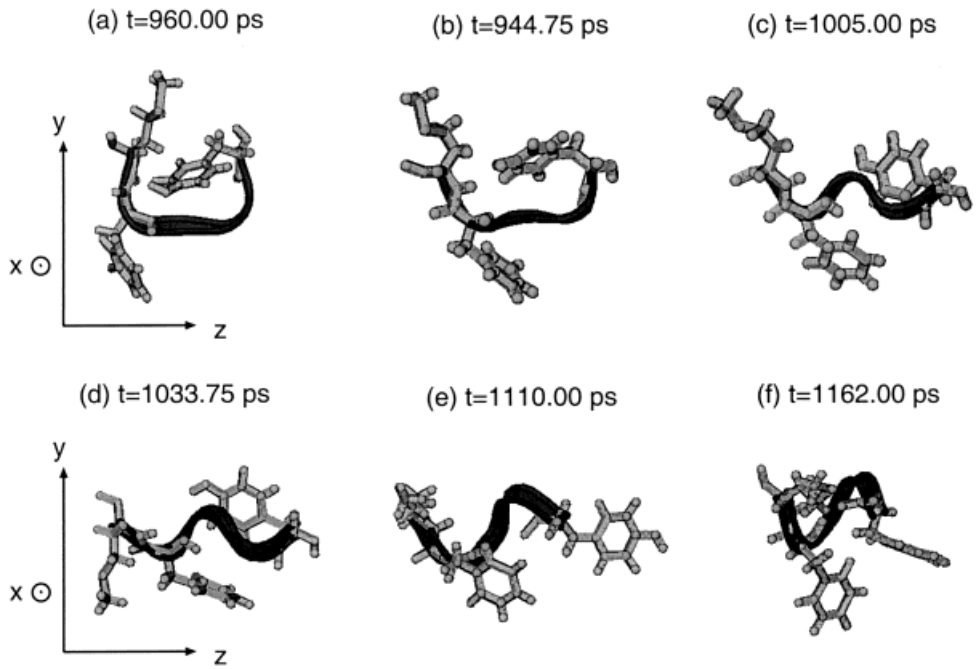

Fig. 12. Time series of the transition between the U-shaped structure III and the α-helix structure I. The backbone is shown in ribbon rendering along with Tyr 1, Phe 4, and NME in licorice rendering using VMD.[37] The axes co-move with the molecule.

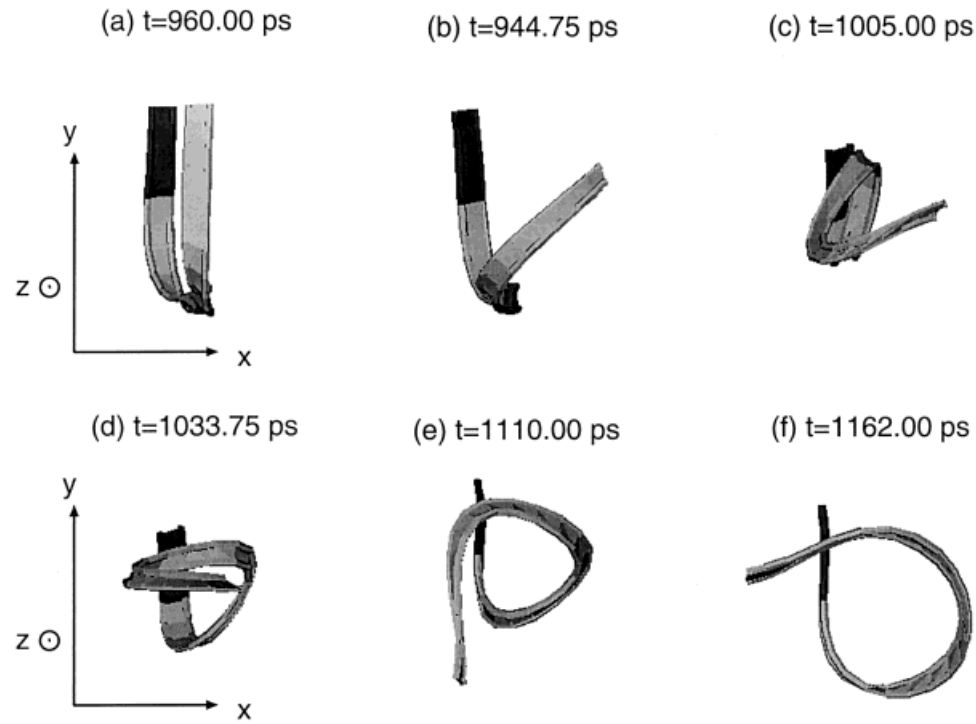

Fig. 13. Time series of the transition between the U-shaped structure III and the α-helix structure I from the perspective looking down the axis of the helix (f).

the U are aligned, only the front arm is visible in Figure 13a. In Figure 13b, the rear arm is now visible, making an angle in the x-y plane with the front arm of approximately 50 degrees, causing the midsection of the backbone to twist.

Compression along the z-axis occurs between t = 994.75 ps and t = 1005 ps. Although difficult to discern from Figure 13, this is clear in Figure 12b,c. As the total extension of the peptide decreases, a kink forms in the midsection. After viewing animations of the trajectory, we

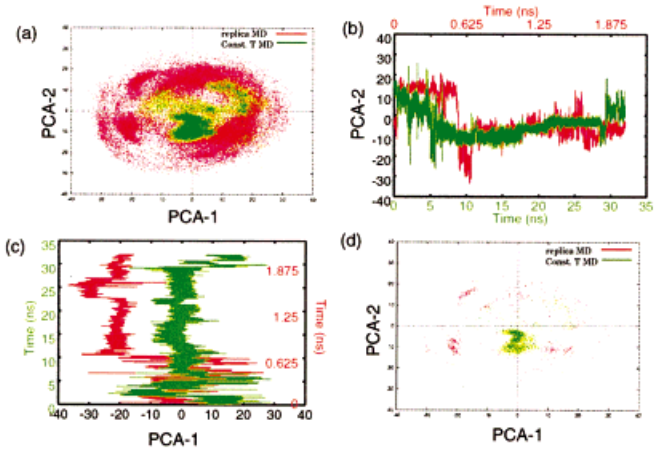

Fig. 14. Comparison of replica exchange (red) and constant temperature molecular dynamics (MD) (green). Each point represents the projection of one configuration in (*PCA*-1, *PCA*-2) space. **a:** Configurations of all temperatures and replicas (1.28×10^5 configurations) and configurations of constant temperature MD (1.28×10^5 configurations). **b:** Trajectory of *PCA*-2. **c:** Trajectory of *PCA*-1. **d:** Configurations of all replicas with target temperature $T = 296$ K (8,000 configurations) and sparse sampling (every 16th configurations) of constant temperature MD (8,000 configurations).

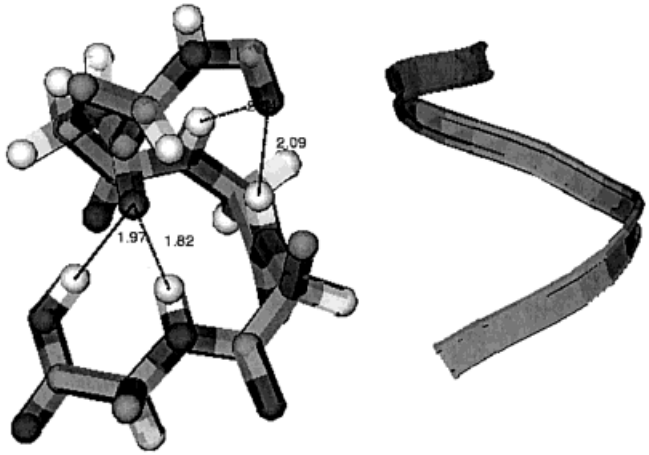

Fig. 15. Dominant configuration of the constant temperature molecular dynamics simulation is not an α-helix, showing hydrogen bonds with one oxygen coupled to two hydrogens.

note that the backbone kinks slightly and then flattens twice (such that the kink is no longer visible) before finally kinking severely at $t = 1{,}005$ ps. This motion was observed to be closely correlated with the motion of Phe 4.

The axial projection of the structure becomes somewhat circular by $t = 1033.75$–1110.00 ps (Fig. 13d,e). Upon further compression and torsion, a well-formed α-helix results by $t = 1{,}162$ ps (Figs. 12f, 13f).

Comparison With Regular Constant Temperature Molecular Dynamics

The control system (a single Met-enkephalin molecule simulated at constant (N, V, T) for 32 ns using constant temperature molecular dynamics for the same parameters as our replica exchange simulations) produced the same number of configurations (1.28×10^5) as our replica exchange simulation. All configurations of the replica exchange simulation and of the constant temperature MD simulation in (*PCA*-1, *PCA*-2) space are shown in Figure 14. The replica exchange simulation covers approximately five times more configurational space than the constant temperature MD simulation, based on the area of the (*PCA*-1, *PCA*-2) plane covered by each simulation. The control peptide appears to be kinetically trapped, close to the transition pathway of the replica exchange simulation discussed above. The dominant configuration of the control peptide is quasi-helical (Fig. 15). Although several hydrogen bonds are formed, these are not the type present in an α-helix. One oxygen appears coupled to two hydrogens.

DISCUSSION

Replica exchange MD simulations of Met-enkephalin in explicit aqueous solution sample helical and nonhelical structures with comparable probabilities. Nonhelical structure IV appears to be a transition structure for transitions between nonhelical structure III and helical structure I (Fig. 7). Detailed study has shown that the transition between the nonhelical U-shaped structure (structure III) and the α-helix structure (structure I) results from simultaneous compression and torsion, as well as from the influence of side-chain motion. The Ramachandran diagrams of our simulations are consistent with those presented for NMR experiments of [Met5]enkephalin-Arg-Phe in aqueous solution at pH 7.68.[9] Our Ramachandran plots differ from those produced by experiments of Graham[4]; however, these experiments were performed at pH 3.87, which could significantly alter the backbone configuration. The presence of helical and nonhelical structures in our simulations is consistent with NMR experiments showing random distributions of conformers.[4,9] Our results are also consistent with the prediction by Li and Scheraga[15] that Met-enkephalin in aqueous solution will be in an unfolded state, with distinct conformations coexisting. Our observation of multiple stable configurations of Met-enkephalin is consistent with the known affinity of Met-enkephalin for distinct opioid receptors (i.e., the μ-, κ-, and δ-opioid receptors). We find the energy barriers between configurations are on the order of $\approx kT$, suggesting that Met-enkephalin switches between configurations with little difficulty.

Other simulations of Met-enkephalin have been performed in vacuo, neglecting the effects of solvent. Sugita and Okamoto[22] presented replica exchange simulations of Met-enkephalin in vacuo, showing Gly 2 Ramachandran plots with structure generally similar to that shown in Figure 4; however, their maxima occurred at $\psi > 0$, while ours exists at $\psi < 0$. Hansmann et al.[17] performed generalized Monte Carlo simulations of Met-enkephalin using a dielectric constant of 2 and force fields, including some implicit water effects. Although the resulting structures were not presented, these simulations did produce energy landscapes with multiple minima at lower temperatures ($150 < T < 300$ K). MD simulations of Met-enkephalin in its zwitterionic form by Perez et al.[14] employed implicit solvent with $\epsilon = r$ and with $\epsilon = 80$[14]. Koca and Carlsen[13] have simulated Met-enkephalin with

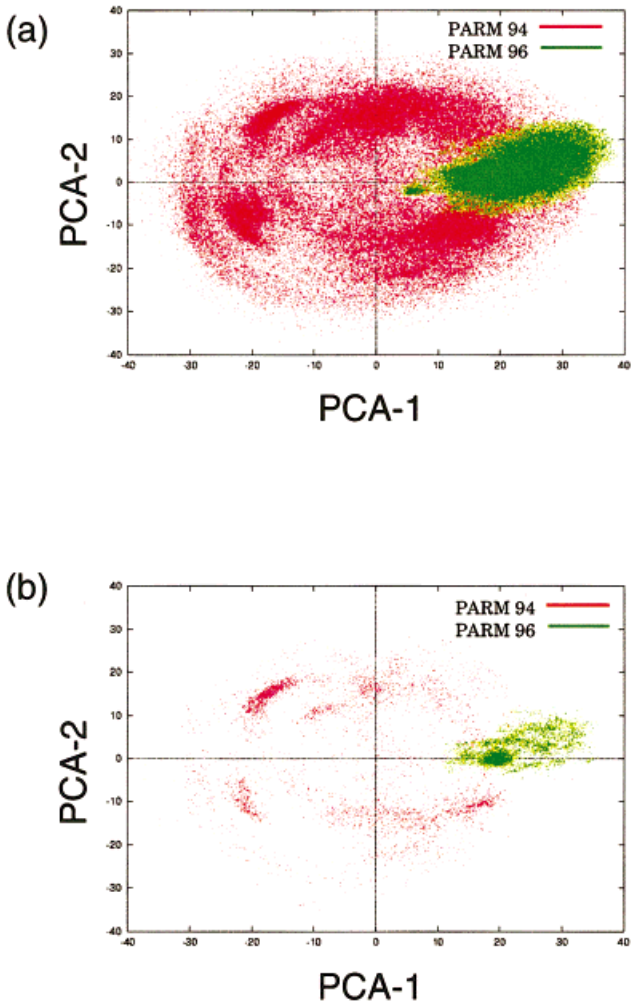

Fig. 16. Comparison of PARM94 (red) and PARM96 (green) force fields. Each point represents the projection of one configuration in (*PCA*-1, *PCA*-2) space. **a:** Configurations of all replicas and all target temperatures. **b:** Configurations with $T = 275$ K only.

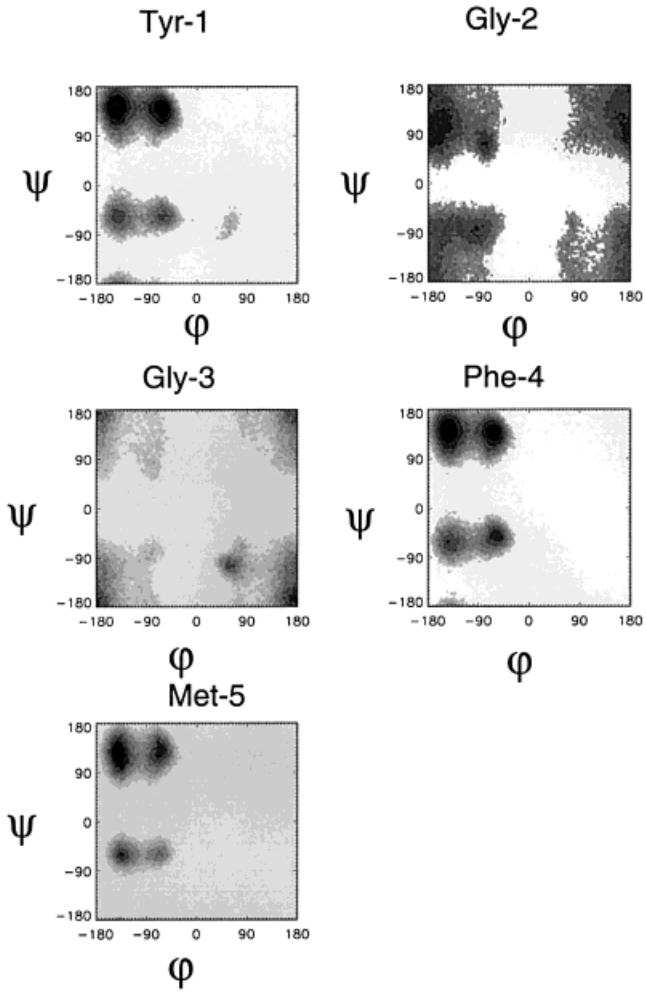

Fig. 17. Ramachandran plots for all five residues of Met-enkephalin, using the PARM96 force field.

implicit solvent and $\epsilon = 78.5$. Both sets of simulations produced configurations with (ϕ, ψ) coordinates consistent with ours. It is difficult to determine the importance of explicit solvent effects, however, as these studies reported less than 40 configurations, in contrast to our 1.28×10^5 configurations.[14] Comparison of our replica exchange simulations with constant temperature MD simulations (Fig. 14) demonstrates that replica exchange MD achieves a significant sampling gain over constant temperature MD, consistent with replica exchange studies of Met-enkephalin in vacuo.[22]

Previous simulations of different pentapeptides have shown similar structures to those produced by our simulations of Met-enkephalin. In particular, constant temperature MD simulations of Tyr-Pro-Gly-Asp-Val show extended, U-shaped, and type II reverse turn structures.[38,39] These simulations displayed a transition pathway of type II turn → U-shaped → extended. The type II turn is similar to our structure IV. Our simulations show the transition U-shaped → turn (structure IV) → helical. While the transition pathways of these two peptides differ, the similarity in structures suggests that there may be limited number of possible structures and transition pathways for pentapeptides (e.g., turn, U-shaped, helix). The transition of U-shaped to helical shown in this work is one possible mechanism of helix nucleation in helix–coil transitions occurring larger proteins.

We have also performed our simulations using the PARM96 force field,[32] which has been optimized to fit ab initio energies calculated for all-α_R and all-β-tetrapeptides in absence of solvent. The only difference between the PARM94 and PARM96 energy parameters is the potential energy term associated with the peptide backbone (ϕ, ψ) dihedral angles:

$$V_{96}[\phi_i, \psi_i) = 0.2(1 + \cos(2\phi_i - \pi)] + 0.4[1 + \cos(4\psi_i - \pi)] + 1.35[1 + \cos(2\psi_i - \pi)] + 0.75[1 + \cos(\psi_i - \pi)]$$

and

$$V_{94}(\phi_i, \psi_i) = 0.3[1 + \cos(2\phi_i - \pi)] + 0.85[1 + \cos(\phi_i)] + 0.3[1 + \cos(2\psi_i - \pi)] + 0.85[1 + \cos(\psi_i)]$$

All other terms in the force fields are identical. If we evaluate the energy differences between the α ($\phi = -\pi/3$, $\psi = -\pi/4$) and extended ($\phi = -\pi/3$, $\psi = 2\pi/3$) for a (ϕ, ψ) pair, we get $\Delta V_{94} = V(\text{ext.}) - V(\alpha) = -0.88$ kcal/mol (in favor of the α conformation), and $\Delta V_{96} = V(\text{ext.}) - V(\alpha) = 1.38$ kcal/mol (in favor of the extended conformation). The bias against the α component in PARM96 is $\approx 3.75\ k_BT$ at 300 K, resulting in the overwhelming sampling of the extended configurations of the PARM96 force field. Figure 16a shows the configurations of all replicas and all target temperatures for the PARM94 and PARM96 simulations projected onto the principle component axes of the PARM94 simulations. Figure 16b displays only the configurations with target temperature $T = 275$ K for all replicas. The PARM96 simulations show configurations only in the nonhelical region of (*PCA*-1, *PCA*-2) space, in between structures III and IV of Figure 6, suggesting a bias toward nonhelical structures for this particular peptide. The Ramachandran diagrams for the PARM96 simulations also display less sampling of helical structures than the PARM94 simulations (Fig. 17). Furthermore, we emphasize that our replica exchange simulations using PARM94 produce Ramachandran diagrams for Gly-3 with ($\phi - \psi$) space structure consistent with that observed in NMR studies.[9] This contrasts with the dramatically different ($\phi - \psi$) space structure produced by the PARM96 simulations.

ACKNOWLEDGMENTS

K.Y.S. thanks K.L. Lagattuta for useful discussions. This work was performed under the auspices of the United States Department of Energy under contract W-740-ENG-36 and the LDRD program at Los Alamos National Laboratory.

REFERENCES

1. Hughes J, Smith TW, Kosterlitz HW, Fothergill LA, Morgan BA, Morris HR. Identification of two related pentapeptides from the brain with potent opiate agonist activity. Nature 1975;258:577–580.
2. Kendrew JC. The encyclopedia of molecular biology. Oxford: Blackwell Science; 1994.
3. Spanagel R, Herz A, Shippenberg TS. Opposing tonically active endogenous opioid systems modulate the mesolimbic dopaminergic pathway. Proc Natl Acad Sci USA 1992;89:2046–2050.
4. Graham WH, Carter ES II, Hicks RP. Conformational analysis of Met–enkephalin in both aqueous solution and in the presence of sodium dodecyl sulfate micelles using multidimensional NMR and molecular modeling. Biopolymers 1992;32:1755–1764.
5. Terenius L. Alcohol addiction (alcoholism) and the opioid system. Alcohol 1996;13:31–34.
6. Rapaka RS, Renugopalakrishnan V, Bhatnagar RS. Am Biotechnol Lab 1985;3:11.
7. Khaled MA, Long MM, Thompson WD, Bradley RJ, Brown GB, Urry DW. Conformational states of enkephalins in solution. Biochem Biophys Res Commun 1976;76:224–231.
8. Spirtes MA, Schwartz RW, Mattice WL, Coy DH. Circular dichroism and absorption study of the structure of methionine–enkephalin in solution. Biochem Biophys Res Commun 1978;81:602–609.
9. D'Alagni M, Delfini M, Di Nola A, Eisenberg M, Paci M, Roda LG, Veglia G. Conformational study of [Met5]enkephalin–Arg–Phe in the presence of phosphatidylserine vesicles. Eur J Biochem 1996;240:540–549.
10. Schiller PW. Fluorescence study on the conformation of a cyclic enkephalin analog in aqueous solution. Biochem Biophys Res Commun 1983;114:268–274.
11. Smith GD, Griffin JF. Conformation of [Leu5]enkephalin from x-ray-diffraction: Features important for recognition at opiate receptor. Science 1978;199:1214.
12. Chew C, Villar HO, Loew GH. Characterization of the bioactive form and molecular determinants of recognition of cyclic enkephalin peptides at the delta–opioid receptor. Biopolymers 1993;33:647–657.
13. Koca J, Carlsen HJ. Conformational behavior and flexibility of met-enkephalin. J Mol Struct 1995;337:17.
14. Perez JJ, Loew GH, Villar HO. Conformational study of Met-enkephalin in its Zwitterionic form. Int J Quantum Chem 1992;44:263.
15. Li Z, Scheraga HA. Monte Carlo–minimization approach to the multiple–minima problem in protein folding. Proc Natl Acad Sci USA 1987;84:6611–6615.
16. Hansmann UHE. Parallel tempering algorithm for conformational studies of biological molecules. Chem Phys Lett 1997;281:140.
17. Hansmann UHE, Okamoto Y, Onuchic JN. The folding funnel landscape for the peptide Met-enkephalin. Proteins 1999;34:472.
18. Berg BA, Neuhaus T. Multicanonical algorithms for 1st order phase-transitions. Physics Letters B 1999;267(2):249–253.
19. Hansmann UHE, Okamoto Y. Prediction of peptide conformation by multicanonical algorithm: New approach to the multiple-minima problem. J Comp Chem 1993;14:1333.
20. Hao MH, Scheraga HA. Monte-Carlo simulation of a first-order transition for protein-folding. J Phys Chem 1994;98:4940.
21. Hukushima K, Nemoto K. Exchange Monte Carlo method and application to spin glass simulations. J Phys Soc Jpn 1996;65:1604.
22. Sugita Y, Okamoto Y. Replica-exchange molecular dynamics method for protein folding. Chem Phys Lett 1999;314:141.
23. Crowley MF, Darden TA, Cheatham TE, Deerfield DW. Adventures in improving the scaling and accuracy of a parallel molecular dynamics program. J Supercomput 1997;11:255.
24. Garcia AE, Sanbonmatsu KY. Exploring the energy landscape of a beta hairpin in explicit solvent. Proteins 2001;42:345–354.
25. García AE, Hummer G. The kinetics of water penetration and escape in proteins. Biophys J 2000;78:P2323.
26. Hummer G, Garde S, García AE, Pratt LR. Water penetration and escape in proteins. Chem Phys 2000;258:349.
27. Garcia AE, Hummer G. Water penetration and escape in proteins. Proteins 2000;38:261–272.
28. Hummer G, Garcia AE, Garde S. Conformational diffusion and helix formation kinetics. Phys Rev Lett 2000;85:2637–2640.
29. Cornell WD, Cieplak P, Bayly CI, Gould IR, Merz KM, Ferguson DM, Spellmeyer DC, Fox T, Caldwell JW, Kollman PA. A 2nd generation force-field for the simulation of proteins, nucleic-acids, and organic-molecules. J Am Chem Soc 1995;117:5179.
30. Pearlman DA, Case DA, Caldwell JW, Ross WS, Cheatham TE, Ferguson DM, Seibel GL, Singh UC, Weiner PK, Kollman PA. AMBER 4.1. San Francisco, CA: University of California; 1994.
31. Berendsen HJC, Postma JPM, van Gunsteren WF, DiNola A, Haak JR. Molecular-dynamics with coupling to an external bath. J Chem Phys 1984;81:3684.
32. Cornell WD, Caldwell JW, Kollman PA. Calculation of the Phi-Psi maps for alanyl and glycyl dipeptides with different additive and non-additive molecular mechanical models. J de Chimie Phys et de Physico-Chimie Biol 1997;94(7-8):1417–1435.
33. Head-Gordon T, Head-Gordon M, Frisch M, Pople JA, Brooks CL. Theoretical-study of blocked glycine and alanine peptide analogs. J Am Chem Soc 1991;113:5989.
34. van der Spoel D, Berendsen HJ. Molecular dynamics simulations of Leu–enkephalin in water and DMSO. Biophys J 1997;72:2032–2041.
35. Garcia AE. Large-amplitude nonlinear motions in proteins. Phys Rev Lett 1992;68:2696–2699.
36. García AE, Blumenfeld R, Hummer G, Krumhansl JA. Multi-basin dynamics of a protein in a crystal environment. Physica D 1997;107:225.
37. Humphrey W, Dalke A, Schulten K. VMD: visual molecular dynamics. J Mol Graph 1996;33:27–28.
38. Tobias DJ, Mertz JE, Brooks CL III. Nanosecond time scale folding dynamics of a pentapeptide in water. Biochemistry 1991;30:6054–6058.
39. Karpen ME, Tobias DJ, Brooks CL III. Statistical clustering techniques for the analysis of long molecular dynamics trajectories: analysis of 2.2–ns trajectories of YPGDV. Biochemistry 1993;32:412–420.